Optics Letters

Ultra-slow light propagation by self-induced transparency in ruby in the superhyperfine limit

Hans Riesen,[1,*] Aleksander Rebane,[2,3,6] Rajitha Papakutty Rajan,[1] Wayne Hutchison,[1] Steffen Ganschow,[4] and Alex Szabo[5]

[1]School of Physical, Environmental and Mathematical Sciences, The University of New South Wales, Canberra ACT 2600, Australia
[2]Physics Department, Montana State University, Bozeman, Montana 59717-3840, USA
[3]National Institute of Chemical Physics and Biophysics, Tallinn, Estonia
[4]Leibniz-Institut für Kristallzüchtung, Max-Born-Straße 2, 12489 Berlin, Germany
[5]Institute for Microstructural Sciences, National Research Council Canada, Ottawa, Ontario K1A 0R6, Canada
[6]e-mail: arebane@montana.edu
*Corresponding author: h.riesen@adfa.edu.au

Received 1 February 2017; revised 10 April 2017; accepted 10 April 2017; posted 12 April 2017 (Doc. ID 285878); published 2 May 2017

Self-induced transparency is reported for circularly polarized light in the $R_1(-3/2)$ line of a 30 ppm ruby (α-Al_2O_3:Cr^{3+}) at 1.7 K in a magnetic field of $B\|c = 4.5$ T. In such a field and temperature, a 30 ppm ruby is in the so-called superhyperfine limit resulting in a long phase memory time, $T_M = 50$ μs, and a thousand-fold slower pulse propagation velocity of ∼300 m/s was observed, compared to the ∼300 km/s measured in the first observation of self-induced transparency (SIT) ∼50 years ago, that employed a ruby with a 500 ppm chromium concentration in zero field and at 4.2 K. To date, this is the slowest pulse propagation ever observed in a SIT experiment. © 2017 Optical Society of America

OCIS codes: (270.5530) Pulse propagation and temporal solitons; (270.1670) Coherent optical effects; (300.6240) Spectroscopy, coherent transient; (300.6250) Spectroscopy, condensed matter.

https://doi.org/10.1364/OL.42.001871

In indirect evidence for Rabi oscillations, McCall and Hahn reported the first observation of self-induced transparency (SIT) by a coherent laser pulse in ruby ∼50 years ago [1–3]. The first report of this remarkable phenomenon led to a wide range of experimental investigations in atomic and molecular gases, metal vapors and transition metal ion and rare-earth-ion-doped crystals, glasses, and fibers [4–19]. Numerous theoretical elaborations were also reported [20–26].

Self-induced transparency (SIT) is based on the coherent interaction of electromagnetic radiation with atoms; in particular, the first part of a coherent light pulse transfers its energy to the atoms and, as long as coherence is maintained, this energy is then re-emitted in phase back into the second half of the pulse. Hence, an intense coherent pulse can render an opaque material completely transparent, and the pulse propagation velocity can be drastically reduced compared to c.

In particular, McCall and Hahn [2] demonstrated that a pulse with a hyperbolic secant shape and a pulse area $\theta = 2\pi$, with θ defined by Eq. (1), can pass an optically dense medium under ideal conditions without any loss:

$$\theta = \left|\frac{\mu_{12}}{\hbar}\int_{-\infty}^{\infty} E(t)\mathrm{d}t\right|. \tag{1}$$

In Eq. (1), μ_{12} is the transition dipole moment between the ground (1) and the excited (2) states, and E is the optical pulse amplitude. Ideal conditions in this context are plane wave, and $T_2^* \ll \tau_p \ll T_2'$, T_1 where τ_p is the pulse length, and $1/T_2^*$, T_2' and T_1 are the inhomogeneous width, the pure dephasing time, and the excited state lifetime, respectively.

McCall and Hahn [1] conducted their experiments at 4.2 K and in zero field with a pink ruby (α-Al_2O_3:Cr^{3+}) of 500 ppm chromium concentration and an inhomogeneous width Γ_{inh} of ∼10 GHz. In some detailed subsequent work on ruby, Asher [27] used a similar sample with $\alpha L \approx 10$ (−44 dB attenuation) within the linear absorption regime $I = I_0 \exp(-\alpha L)$.

In this Letter, we have reinvestigated the SIT phenomenon in a ruby doped with 30 ± 2 ppm chromium (Cr/(Cr + Al)) that was grown along the crystal c-axis by the Czochralski method. The raw material, a mixture of pre-melted Al_2O_3 granules with a purity of better than 4N, and an appropriate amount of ruby single crystal was melted in an inductively heated iridium crucible surrounded by zirconia and alumina thermal insulation. The crystal was pulled on an [001] oriented sapphire seed in a nitrogen atmosphere with the addition of 0.3 vol. % CO_2. Such a gas mixture yields an oxygen activity at the growth temperature of approximately 2×10^{-4} bar, resulting in a chromium distribution coefficient near unity [28]. Additionally, to further improve the homogeneity of the dopant distribution in the crystal, the pulling rate was continuously reduced from 2.0 mm/h to 1.0 mm/h along the cylindrical part of the crystal. After the growth was completed, the crystal was extracted from the melt and cooled to room temperature within 15 h. The crystal was cut to a length of 7.27 mm, and the two

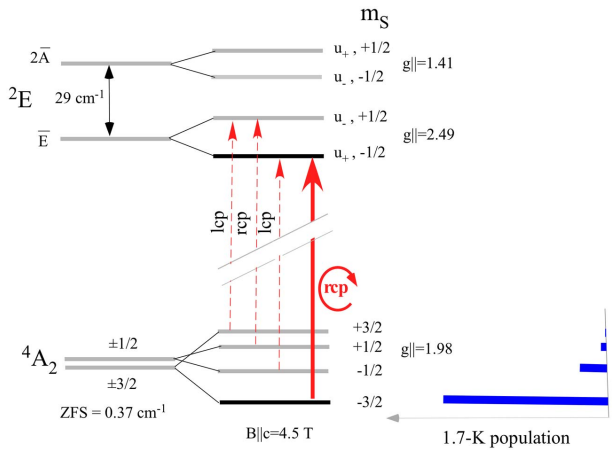

Fig. 1. Schematic energy level diagram for the $^4A_2 \rightarrow {}^2E$ transitions of a ruby in $B\|c = 4.5$ T. Zero field splittings, g-factors, and circular polarizations [29] for the transitions to the lower ^2E level are indicated.

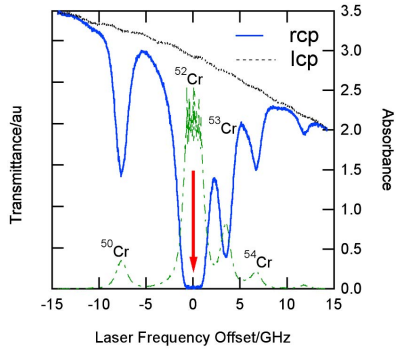

Fig. 2. Transmission spectra in the region of the $^4A_2(-3/2) \rightarrow \bar{E}(-1/2)$ transition $[R_1(-3/2)]$ for the 7.27 mm Czochralski ruby in $B\|c = 4.5$ T and $T = 1.7$ K along the c-axis with lcp and rcp light. The corresponding rcp absorption spectrum (green trace) is limited to an absorbance of 2.5 by the 20 dB isolation of the polarizer quarter-wave plate combination. The transitions are assigned to the isotopes.

faces perpendicular to the crystal c-axis were polished to allow α-polarized (light propagating along the c-axis) experiments.

Whereas SIT was measured in zero field in the early work, we have applied an external magnetic field $B\|c = 4.5$ T. In such a field, the schematic energy diagram shown in Fig. 1 applies, and the $^4A_2$ $m_S = \pm 3/2$ and $m_S = \pm 1/2$ zero field Kramers doublets, split by

$$E_{m_s} = \pm m_s \mu_B g_\| B\|c, \tag{2}$$

where μ_B is the Bohr magneton, and $g_\| = 1.987$ is the g-factor of the $^4A_2$ ground state. The same equation can be used for the excited states with the lower ^2E level, $\bar{E}$ (^2E), having an effective $g_\|$ factor of 2.49 [29]. In this case, the large deviation from spin-only behavior is due to unquenched orbital momentum in the trigonal quantization direction.

As can be seen from Fig. 1, the Cr(III) ions predominantly populate the $^4A_2(-3/2)$ spin level (~84%) in $B\|c = 4.5$ T and at 1.7 K. As a consequence, the $R_1(-3/2)$ transition between this level and the $\bar{E}(-1/2)$ level of the ^2E excited state provides a near perfect two-level atom system. Importantly, under these conditions, ruby is in the so-called superhyperfine limit. In contrast to the zero field experiments at 4.2 K, direct and indirect electron-spin-electron-spin flipping are negligible, and dephasing is governed by the interaction of the electron spin of Cr(III) (guest) with the ^{27}Al nuclear spins (host) [30]. These Al nuclear spins are detuned from the bulk in the vicinity of the $-3/2$ electron spin due to the large magnetic moment of the latter. This leads to the so-called frozen core effect, where the flip rate of the nuclear spins decreases with decreasing distance from the electron spin. As a consequence, nuclear spins well separated from the electron spin flip first, followed by flips in the nearer neighborhood. This leads to an increase in the optical line width as time progresses i.e., the homogeneous line width becomes ill defined. For example, as a consequence the time dependence of photon echoes becomes non-exponential as the dephasing rate increases with time [31,32], and the decay of the echo can be described by

$$I = I_0 \exp[-(4\tau/T_M)^x], \tag{3}$$

where T_M is a phase memory time. For $x = 1$, T_M is equal to the transverse dephasing time T_2 $(1/T_2 = 1/2T_1 + 1/T_2')$.

For the $R_1(-3/2)$ transition in ruby, T_M was determined to be 50 μs and $x = 2.4$ [31,33]. Importantly, all transitions are circularly polarized in $B\|c$, as shown in Fig. 1. The $R_1(-3/2)$ transition under consideration in this Letter is right circularly polarized (rcp) and, hence, it is straightforward to generate a reference signal by using left circularly polarized (lcp) light. This is corroborated by the data displayed in Fig. 2, where the transmission spectra of rcp and lcp in the region of the $R_1(-3/2)$ transition are shown.

For these spectra, the laser was scanned around 693.4117 nm by ±15 GHz by using the setup shown in Fig. 3, but without modulating the amplitude of the laser beam (i.e., an unmodulated zeroth order is used) and scanning the Toptica DL100 external cavity diode laser (ECDL) frequency by a Toptica Digilock controlyzer. For changing from rcp to lcp light, the quarter-wave plate was turned by 90 deg (see also text below). The rcp absorption spectrum (calculated from the transmission spectra) is also shown in Fig. 2; the absorbance is limited to ~2.5 because of the limited circular polarization (~20 dB) of the polarizer quarter-wave plate combination employed. By measuring the circularly polarized transmission spectra of a 1 mm thick crystal along the c-axis in a low magnetic field of 0.093 T (not illustrated here), we extrapolated the absorbance A of the 7.27 mm thick crystal to be 6.2 ± 0.2 for the $R_1(-3/2)$ transition of ^{52}Cr in $B\|c = 4.5$ T and 1.7 K. Using the absorption spectrum in Fig. 2, a Gaussian line shape can be fitted to this transition for the ^{52}Cr isotope, and a value of $A = 6.3 \pm 0.2$ results in accord with this extrapolation and the isotope ratios. We note here that the inhomogeneous line width of the $R_1(-3/2)$ transition in the present Czochralski crystal is $\Gamma_{inh} = 1.4 \pm 0.1$ GHz, indicating a very high quality of the crystal and enabling the current SIT experiment as it renders a high OD. This width compares well with a previously reported value of 1.2 GHz that was measured in a much smaller volume [34]. In the present case, the slightly larger Γ_{inh} is most likely due to (probe volume dependent) macroscopic strain broadening. The main components of the SIT experiment are illustrated in Fig. 3. The beam of the ECDL was modulated by an 80 MHz acousto-optic modulator (Isomet 1205C-1 with 222A-1 AOM driver, gated by a Tektronix AFG3102). The resulting square pulses of 3–9 μs duration with ~0.2 μs rise

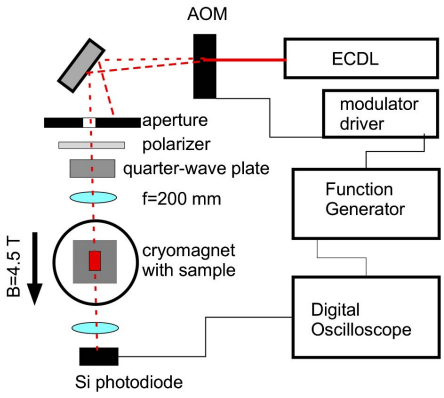

Fig. 3. Schematic diagram of the SIT experiment. The light of an ECDL (Toptica DL100) was modulated by a 80 MHz acousto-optic modulator (Isomet 1205C-1). The sample was kept at 1.7 K in a cryomagnet with a magnetic field $B \| c = 4.5$ T.

and fall times were circularly polarized and then focused by a 200 mm lens onto the ruby crystal that was mounted with its c-axis in the direction of the magnetic field and the propagation direction of the light in a 5 T cryomagnet (BOC).

The cross section of the laser beam was approximately Gaussian with a waist (at $1/e^2$) and a FWHM of ~290 and ~170 μm, respectively, at the center of the sample as determined by both a CCD camera and a beam profiler (Thorlabs WM100 Omega Meter). The power of the square input pulses was 0.76 mW and, hence, a power density of ~1.2 W/cm^2 was employed. The pulses were detected by a fast photodiode (Thorlabs PDA 10A) and accumulated on a digital oscilloscope (LeCroy waveSurfer 422). The transmitted pulse was observed for lcp and rcp light, and the repetition rate was chosen at 1 Hz to allow the spin system to fully relax. The SIT results obtained are shown in Fig. 4. Since lcp light is not absorbed by the $R_1(-3/2)$ line, the dashed (green) waveform in Fig. 4 can serve as the (non-attenuated) reference pulse. As discussed above, the rcp light is not perfectly polarized and contains ~1% of lcp light; this 1% component is clearly visible as the leading square pulse that coincides with the data obtained for lcp light, but at ~100 × reduced amplitude. It is noted here that the optical density of the sample $A = 6.2$ is too high for this first component to be transmitted rcp light. It can be seen in Fig. 4 that there is a sharp onset of a delayed second pulse when the pulse width exceeds 3.5 μs. The amplitude of this second pulse keeps rising, and the delay becomes shorter with longer input pulses. For example, whereas the transmitted energy is ~1% of the incident pulse for a 3.5 μs pulse, it rises to ~16% for a 9 μs pulse, while the delay gets reduced from ~24 to ~1.2 μs, respectively. By solving the Maxwell–Bloch equations, McCall and Hahn [2] showed that, in SIT, pulses $>\pi$ evolve into 2π pulses with a hyperbolic secant shape. In the present experiments, the amplitude of the square pulses was constant and, hence, the pulse area θ is simply proportional to the pulse width.

A summary of the observed delay of the transmitted rcp pulse (peak maximum of delayed pulse) as a function of the pulse width is compared in Fig. 5 with data reported in the early work of Asher [27]; the latter is shown versus the pulse area θ.

The qualitative behavior for the two sets of data is very similar, but on vastly different time scales (μs versus ns). From the comparison in Fig. 5, we can also conclude that, in our experiments, a pulse width of 3.5 μs corresponded to an area θ of ~π. In the present experiment, the ruby sample was in the superhyperfine limit with a much longer dephasing time. This explains the much larger delay, as much longer incident pulse times are possible. The inset of Fig. 5 is a plot of the ratio of the energy of the rcp to the non-attenuated lcp pulse. The lower than unity maximum transmission, as well as the observed asymmetric temporal pulse shapes in Fig. 4, are both quantitatively explained by the nearly Gaussian incident spatial beam profile. Because the intensity was higher at the center of the beam, the corresponding effective pulse area was higher compared to that at the periphery of the beam cross section. Indeed, at the short pulse durations the pulse area was only large enough to achieve SIT at the center of the beam, whereas

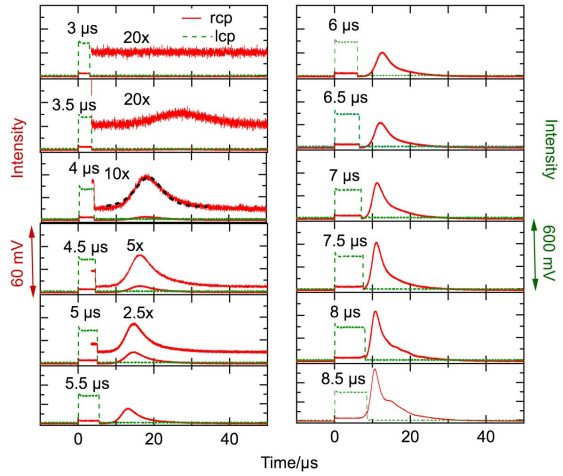

Fig. 4. Self-induced transparency in the $R_1(-3/2)$ transition of ruby at 693.4117 nm in $B \| c = 4.5$ T and at 1.7 K. The dashed (green) and solid (red) traces show the transmitted light signal for lcp (right-hand y-scale) and rcp (left-hand y-scale) light, respectively. The pulse width is indicated. The dashed black line for the 4 μs experiment is a fit using a hyperbolic secant.

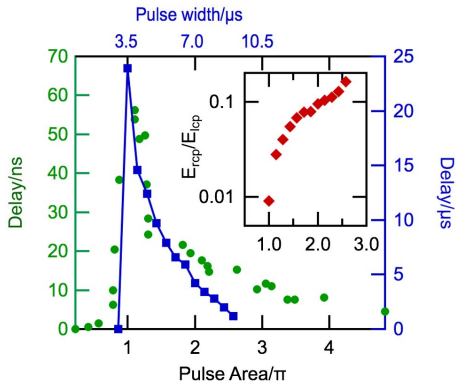

Fig. 5. Comparison of observed pulse (rcp) delays in the $R_1(-3/2)$ line (blue squares, right-hand y-axis in microseconds) with values (solid green circles, left-hand y-axis in nanoseconds) reported for ruby in early work [27]. The insert shows the output-energy ratio of the rcp pulse to the (non-attenuated) lcp pulse. The top x-axis scale applies for the data of this Letter.

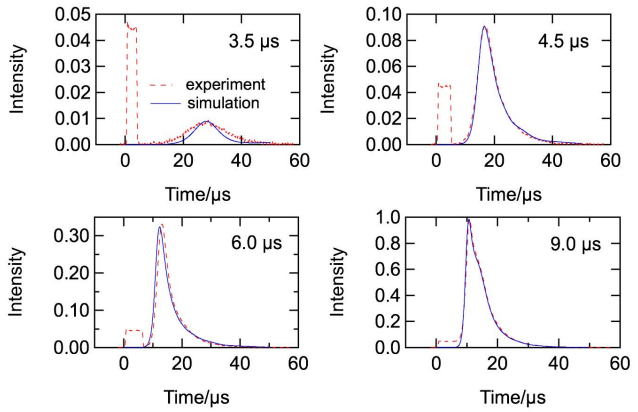

Fig. 6. Comparison of the calculated (blue solid line) and experimental (red dashed line) SIT pulse profiles transmitted through the sample for selected pulse widths as shown. Simulation parameters used: $T_2 = 50$ μs, $T_1 = 10$ ms, $\alpha L = 14.5$.

in the rest of the incident pulse cross section, where the minimum required pulse area was not satisfied, the incident pulse energy was dissipated into the sample. The transmitted fraction of the beam increased with increasing pulse duration, but each section still propagated according to its own characteristic effective pulse area. This spread of the pulse area values caused the stretched-out temporal profile of the pulse. To quantitatively describe these effects, we simulated the transmission of a square incident pulse with a range of pulse energy values and pulse durations using the optical Bloch equations [35,36]:

$$\frac{d}{dt}u = \Delta v - \frac{u}{T_2},$$
$$\frac{d}{dt}v = -\Delta u - \frac{v}{T_2} + 2\Omega w,$$
$$\frac{d}{dt}w = -\frac{w+1}{T_1} - 2\Omega v, \tag{4}$$

where u and v are the in- and out-of-phase components of the induced polarization, respectively, w is the population inversion, E is the optical amplitude, Δ is the frequency detuning, and $\Omega = |\mu_{12}E/\hbar|$ is the Rabi frequency (T_2 and T_1 are defined above).

To simulate the SIT effect, the sample was divided into 250 equal thickness layers, each corresponding to the absorption coefficient, $\alpha L = 0.058$, with the assumption that the amplitude transmitted through one thin slice serves as the input pulse amplitude for the next slice. The calculated pulse shapes for a few selected pulse durations are shown in Fig. 6, where we combined up to 15 different pulse amplitudes to emulate the distribution of effective pulse areas in a Gaussian beam profile. The simulation reproduces both the observed delay, as well the asymmetric shape of the SIT pulse remarkably well, thus confirming that the shape of the transmitted optical signal is determined by the incident pulse area, rather than by the incident pulse shape. In this context, it is interesting to note that this apparent loss of the information may be reversible, at least on the time scale of T_2, i.e., as long as the quantum coherence of the medium is retained. This Letter shows that remarkable control over light pulse propagation can be exercised by the SIT effect via circular polarization, high magnetic field, and the width of the incident pulse; such control is important in all-optical communication and computing. Hence, further detailed studies of the SIT effect in the solid state are warranted; in particular, the effect should be studied with shorter pulse lengths, but higher pulse amplitudes, and effects such as counter-propagating solitons could be explored [37].

REFERENCES

1. S. L. McCall and E. L. Hahn, Phys. Rev. Lett. **18**, 908 (1967).
2. S. L. McCall and E. L. Hahn, Phys. Rev. **183**, 457 (1969).
3. S. L. McCall and E. L. Hahn, Phys. Rev. A **2**, 861 (1970).
4. C. K. N. Patel and R. E. Slusher, Phys. Rev. Lett. **19**, 1019 (1967).
5. L. M. Peterson, Appl. Phys. Lett. **31**, 86 (1977).
6. S. S. Alimpiev and N. V. Karlov, Sov. Phys. JETP-USSR **34**, 947 (1972).
7. C. D. David and W. M. Clark, Appl. Phys. Lett. **23**, 306 (1973).
8. W. Krieger, G. Gaida, and P. E. Toschek, Z. Phys. B **25**, 297 (1976).
9. G. Xu and T. A. King, Phys. Rev. A **30**, 354 (1984).
10. R. E. Slusher and H. M. Gibbs, Phys. Rev. A **5**, 1634 (1972).
11. K. Masuda, C. Affolderbach, G. Mileti, J. C. Diels, and L. Arissian, Opt. Lett. **40**, 2146 (2015).
12. J. H. Yi, H. M. Park, Y. J. Rhee, and J. M. Lee, Jpn. J. Appl. Phys. **139**, 1128 (2000).
13. W. K. Lee, M. K. Oh, W. S. Choi, J. H. Jeon, J. H. Lee, and J. S. Chang, Jpn. J. Appl. Phys. **141**, 5170 (2002).
14. G. J. Salamo and H. M. Gibbs, B. Am. Phys. Soc. **17**, 1200 (1972).
15. D. J. Bradley, G. M. Gale, and P. D. Smith, Nature **225**, 719 (1970).
16. A. Szabo and N. Takeuchi, Opt. Commun. **15**, 250 (1975).
17. V. V. Samartsev and R. G. Usmanov, Zh. Eksp. Teor. Fiz. **72**, 1702 (1977).
18. M. Nakazawa, Y. Kimura, K. Kurokawa, and K. Suzuki, Phys. Rev. A **45**, R23 (1992).
19. A. I. Maimistov and A. M. Basharov, Izv. Akad. Nauk. Fiz. **62**, 354 (1998).
20. R. K. Bullough, P. J. Caudrey, J. C. Eilbeck, and J. D. Gibbon, Opto-Electronics **6**, 121 (1974).
21. E. I. Bogdanov, V. R. Nagibarov, and I. A. Nagibarova, Zh. Eksp. Teor. Fiz. **77**, 498 (1979).
22. A. Leclair, Nucl. Phys. B **450**, 753 (1995).
23. A. I. Maimistov, A. M. Basharov, S. O. Elyutin, and Y. M. Sklyarov, Phys. Rep. **191**, 1 (1990).
24. A. I. Maimistov and S. O. Elyutin, Chaos Solitons Fractals **8**, 369 (1997).
25. F. A. Hopf and M. O. Scully, Phys. Rev. B **1**, 50 (1970).
26. M. O. Scully, G. S. Agarwal, O. Kocharovskaya, V. V. Kozlov, and A. B. Matsko, Opt. Express **8**, 66 (2001).
27. I. M. Asher, Phys. Rev. A **5**, 349 (1972).
28. S. Ganschow, D. Klimm, and R. Bertram, J. Cryst. Growth **325**, 81 (2011).
29. I. Trabjerg and H. U. Gudel, Acta Chem. Scand. A **28**, 8 (1974).
30. A. Szabo, T. Muramoto, and R. Kaarli, Phys. Rev. B **42**, 7769 (1990).
31. J. Ganem, Y. P. Wang, D. Boye, R. S. Meltzer, W. M. Yen, and R. M. Macfarlane, Phys. Rev. Lett. **66**, 695 (1991).
32. A. Szabo, J. Lumin. **58**, 403 (1994).
33. S. H. Huang and A. Szabo, J. Lumin. **68**, 291 (1996).
34. P. E. Jessop and A. Szabo, Opt. Commun. **33**, 301 (1980).
35. R. W. Boyd, *Nonlinear Optics*, 3rd ed. (Elsevier, 2008).
36. G. S. He, *Nonlinear Optics and Photonics* (Oxford University, 2015).
37. A. Pusch, J. M. Hamm, and O. Hess, Phys. Rev. A **82**, 023805 (2010).